ELSEVIER

Thin Solid Films 260 (1995) 26-31

thin solid films

Sputtered molybdenum bilayer back contact for copper indium diselenide-based polycrystalline thin-film solar cells

John H. Scofield[a,*], A. Duda[a], D. Albin[a], B.L. Ballard[b], P.K. Predecki[b]

[a]National Renewable Energy Laboratory, 1617 Cole Blvd., Golden, CO 80401, USA
[b]University of Denver, Department of Engineering, 2390 So. York, Denver, CO 80208, USA

Received 26 May 1994; accepted 15 November 1994

Abstract

A method is described for fabricating low-resistivity molybdenum films on soda-lime glass substrates with good adhesion. Films are sputtered onto substrates nominally held at room temperature in a cryo-pumped d.c. magnetron system in a partial pressure of argon. 1-μm-thick films sputtered at low argon pressure were found to have low resistivity (10–15 μΩ cm), were under compressive stress, and suffered from poor adhesion. Films sputtered with high argon pressure had high resistivity (50–250 μΩ cm), were under tensile stress, but adhered well to the glass. By varying argon pressure during deposition, 1-μm-thick molybdenum bilayers have been fabricated with both low resistivity (12–14 μΩ cm) and good adhesion. These films are being used as back contacts for the National Renewable Energy Laboratoy's state-of-the-art polycrystalline copper indium gallium diselenide solar cells with good results.

Keywords: Molybdenum; Resistivity; Sputtering; Stress

1. Introduction

Copper indium diselenide, $CuInSe_2$ (CIS), and its gallium alloys, $Cu(In_{1-x}Ga_x)Se_2$ (CIGS), have emerged as promising polycrystalline thin-film semiconductors for solar cell absorber layers [1]. These direct bandgap semiconductors have bandgaps ranging from 1.0 to 1.26 eV, and have been used as absorber layers in small-area solar cells having total-area efficiencies of up to 16.4% [2], the highest for any polycrystalline thin-film photovoltaic (PV) technology.

Solar cells fabricated at the National Renewable Energy Laboratory (NREL) have the structure shown in Fig. 1. A 1-μm-thick Mo back contact layer is deposited onto glass substrates. The nominally 2.5-μm-thick p-type CIS or CIGS absorber layer is subsequently deposited onto the Mo-coated glass at temperatures ranging from 450 °C to 590 °C, depending on the deposition process. The window layer, deposited over the absorber layer, consists of a 50-nm-thick, near-intrinsic, chemically grown CdS layer followed by an ion-beam-sputtered, lightly doped (50 nm) then heavily doped (300 nm), n-type ZnO layer. An Al–Ni

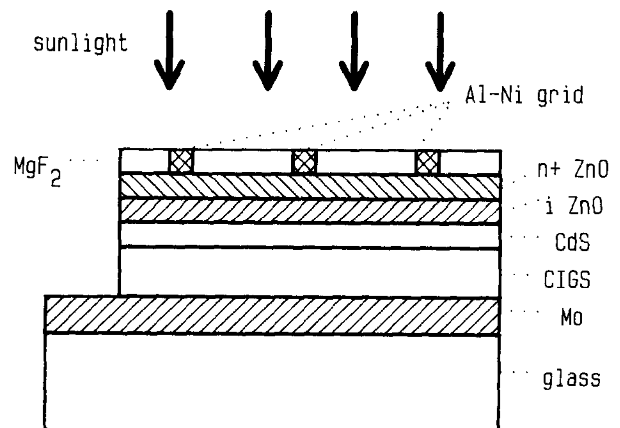

Fig. 1. Cross-sectional view of the CIS or CIGS solar cell structure (not to scale).

*Permanent address: Department of Physics, Oberlin College, Oberlin, OH 44074, USA.

0040-6090/95/$9.50 © 1995 — Elsevier Science S.A. All rights reserved
SSDI 0040-6090(94)06462-8

grid is fabricated on top of the window layer to form the top contact. A MgF_2 anti-reflection coating is deposited over the finished device. Test devices have a nominal total area of 0.43 cm^2. The details of the cell fabrication are found elsewhere [3].

While the details vary, CIS and CIGS cells generally have structures similar to the NREL cells described above. In particular, Mo is nearly always used for the back contact layer. The reason for this is partially historic and partially scientific. A variety of metal/CIS contacts have been investigated, including Mo [4–8], Pt [4,5,8], Au [4–6,8,9], Au/Be [4], Al [6,10,11], Ni [6,7,9], Ag [6], and Cu [6]. These studies show that Pt, Ni, Au, and Mo all form fairly reproducible, low-resistance contacts to CIS. With annealing at elevated temperatures, Au and Pt show significant diffusion into the CIS [5], while Mo and Ni contacts seem to improve with high-temperature treatment [9]. Other evidence shows that both Mo and W films deposited on CIS interdiffuse with the CIS at 600 °C [12].

In these investigations, however, the metal layers were deposited onto either single-crystal or polycrystalline CIS at relatively low temperatures. The contact properties of CIS films formed at high temperatures on metallic thin films are likely to be quite different. Moreover, for polycrystalline CIS solar cells, the metallic back contact forms the substrate upon which the absorber layer is formed. Because of its relative stability at the processing temperatures, resistance to alloying with Cu and In, and its low contact resistance to CIS, Mo has emerged as the dominant choice for the back contact layer to CIS and CIGS solar cells.

A number of papers have been written on the properties of sputtered Mo films [13–22]. Like other refractory metals deposited with d.c.-magnetron sputtering, a correlation is observed between the sputter gas pressure and the stress of the as-deposited film [13–16]. Films deposited with low Ar pressure are generally found to be under compressive stress, while those deposited with high pressures are found to be under tensile stress. (Of course, the scale for high and low pressure is determined by the particular sputter system and target geometry.) Gross stress may be determined by visual inspection in that highly compressed films tend to buckle up, frequently in zigzag patterns, whereas films under extreme tensile stress develop a system of stress lines that look like scratches.

In this work, the results of adhesion, sheet resistivity, and biaxial stress measurements on a set of seven thin Mo films deposited at various Ar pressures are reported. The sputtered film's growth microstructure was used as a model to understand the changing stress state of the film with gas pressure, and served as a rationale for the bilayer method developed here. The details of the model employed and the stress measurements are described in a forthcoming publication [17].

2. Experimental procedures

2.1. Film fabrication

A series of seven Mo films were prepared under identical conditions except for variation in the Ar pressure during sputtering. Films were sputter-deposited onto 5 cm × 5 cm × 2.4 mm soda-lime glass substrates held approximately 8 cm from a 12 cm × 20 cm, planar, d.c. magnetron, Mo target in a high-vacuum system (chamber volume ≈ 80 l) evacuated by a CT-8 cryopump. Films were deposited simultaneously onto two substrates without rotation. The long axis of the nominally 5 cm × 10 cm substrate combination was aligned and centered above the long axis of the rectangular sputter target.

The following procedure was used for depositing all films. First, the chamber was evacuated to a base pressure close to 1×10^{-6} Torr. Next, with the high-vacuum valve fully open, Ar flow into the chamber was increased until the chamber pressure rose to 0.2 mTorr, as measured by a Granville–Philips model 275 convectron gauge calibrated for Ar. Third, the gate-valve was throttled to raise the chamber pressure to a value p to be maintained during deposition. Fourth, the high voltage to the d.c. power supply was turned on, and the current control rapidly increased until the current I was 1.0 A. During the duration of the sputter process (8–10 min) the gate-valve and current control were manually adjusted as necessary to maintain constant pressure and current. The voltage was recorded after it stabilized, about 1 min into the deposition. Each film was deposited at (nominally) room temperature with a sputter current of 1.0 A. Based on calibration runs (see below), the sputter time for each pressure was chosen to yield a film having a nominal thickness of 500 nm. The deposition parameters are summarized in Table 1.

2.2. Film thickness and resistance measurements

Sample thicknesses were not measured directly. Instead, calibration films were deposited for 5.0 min with

Table 1
Summary of deposition parameters for the samples of this study. Listed are the Ar pressure (p), voltage (V), film thickness (t), and deposition rate (R). The sputter current $I = 1.0$ A for all films

p (mTorr)	V (V)	t (nm)	R (Å s^{-1})
0.2	340	540	10.0
0.5	340	460	9.2
1.0	330	520	9.6
2.0	315	500	9.3
5.0	310	500	8.3
10.0	262	470	9.8
20.0	240	620	10.3

a given sputter current and Ar pressure. The thickness of each calibration film was determined (see below) and the sputter rate calculated by dividing this by the known sputter time. It was then assumed that the sputter rate was the same for subsequent runs for the same p and I. Numerous checks were made to determine film uniformity and reproducibility.

The thickness of a calibration film was determined as follows. A liquid paste was used to "paint" a series of approximately 2 mm × 2 mm "dots" onto the surface of a cleaned glass substrate. After allowing the dots to dry the substrate was loaded into the deposition chamber. A thin Mo film was subsequently sputtered onto the substrate at the desired Ar pressure for a known amount of time, typically 5 min. The substrate was subsequently removed from the chamber and the dot pattern transferred to the Mo film by dissolving away the paste by soaking the substrate in an organic solvent using an ultrasonic cleaner for a few minutes. Film thicknesses were then determined at all locations where the dots had been, using an Tencor thin-film profilometer.

Film sheet resistance was determined at several locations on each film using a standard four-probe technique. Sheet resistances varied by no more than 10% across the 5 cm × 10 cm substrate area.

2.3. X-ray biaxial stress determination

Preliminary Bragg–Brentano X-ray diffraction (XRD) measurements were performed on the seven films using a Rigaku instrument and Cu Kα radiation. These XRD measurements may be used to approximate one component of the strain tensor, i.e. perpendicular to the plane of the film. To deduce in-plane film stress, however, back-reflection measurements at several sample tilt angles are required.

Such measurements of the Mo 321 peak profiles at ~132° 2Θ were made on a Siemens D-500 diffractometer using SOCABIM DIFFRACT-AT software. The diffractometer was configured with parallel beam optics (0.1° divergence slit, 0.4° receiving Soller slit) and a Kevex solid state energy dispersive detector. X-rays were generated from a Cu tube and the detector window was tuned to Kα radiation, $E = 8.04$ keV.

The Mo 321 peaks were fitted using a pseudo-Voigt function to accurately determine the Kα_1 peak positions. The X-ray elastic constants used were the average of the Voigt and the Reuss values: $S_1 = -0.9799 \times 10^{-6}$ MPa^{-1}, $1/2S_2 = 4.1798 \times 10^{-6}$ MPa^{-1}. Because the anisotropy coefficient for Mo is small ($S_0 = 0.102 \times 10^{-6}$ MPa^{-1}) [23], the films were assumed to be elastically isotropic.

In each of the seven samples, an in-plane biaxial stress state was assumed. Previous studies indicated that, in magnetron-sputtered Mo films, these stresses are not equibiaxial [16,24]. It has been found that the orientation of the film's substrate to the magnetron cathode axis influences the stress magnitude. The regular $\sin^2\psi$ technique [25] was employed to evaluate the in-plane stresses in directions parallel and perpendicular to the cathode's oval racetrack axis.

3. Results and discussion

The dependency of the room-temperature electrical resistivity on sputter gas pressure is listed in Table 2 and graphed in Fig. 2. From an electrical point of view, one desires the lowest sheet resistance possible for the back contact of a solar cell, minimizing its contribution to the series resistance of the cell. For films in our study, this is accomplished by sputtering at the lowest Ar pressure. (Our gas flow and pressure control was not reliable for $p < 0.2$ mTorr, so we did not attempt to sputter films at lower pressures. Moreover our data suggested that little improvement in resistivity would be

Table 2
Summary of electrical properties, results of adhesion tests, and X-ray measurements for sputtered Mo films. Listed are the Ar pressure (p); electrical properties sheet resistance (r_{sh}), and resistivity (ρ); success or failure of tape test for adhesion; and GIXRD data in-plane stress parallel to (σ_{11}) and normal to (σ_{22}) cathode axis

Film p (mTorr)	Electrical r_{sh} (Ω □$^{-1}$)	ρ (μΩ cm)	Adhesion tape test	Stress σ_{11} (MPa)	σ_{22} (MPa)
0.2	0.2	10.8	fail	−316	−505
0.5	0.26	12.0	fail	61	−231
1.0	0.24	12.5	fail	577	370
2.0	0.25	12.5	pass	1141	1028
5.0	0.66	33	pass	364	474
10.0	1.44	68	pass	−7	22
20.0	4.1	250	pass	−160	−167

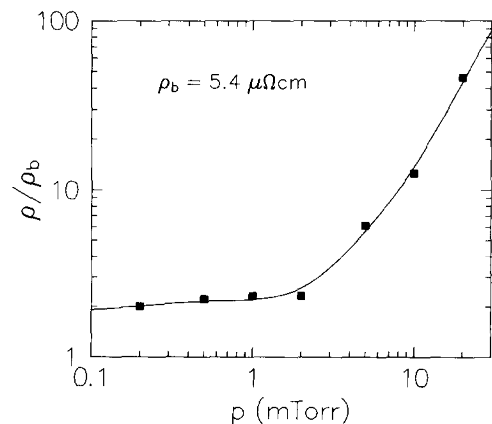

Fig. 2. Graph of the normalized, room-temperature film resistivity, ρ/ρ_b, versus Ar pressure during sputtering. The curve is a guide to the eye.

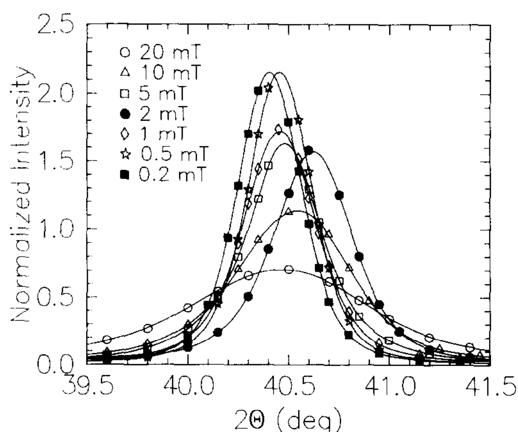

Fig. 3. XRD profiles of the 110 reflection for the various films (Bragg–Brentano geometry). Curves are normalized to have the same area under all peaks. X-ray diffraction measurements were performed using Cu Kα radiation.

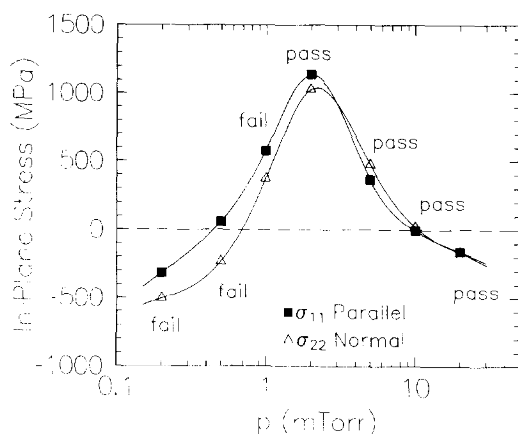

Fig. 4. In-plane stresses plotted against Ar pressure; negative values indicate compression while positive values indicate tension. ■, stress parallel to, and △ perpendicular to, the cathode axis. The solid curves are guides to the eye. Tape test results for adhesion are also indicated.

achieved by sputtering at lower pressures.) Our lowest resistivity films, sputtered with $p = 0.20$ mTorr, had a resistivity of 10.5 μΩ cm, roughly twice the room-temperature bulk value, $\rho = 5.4$ μΩ cm.

The results of the X-ray measurements are summarized in Table 2 and Figs. 3 and 4. Examples of the Bragg–Brentano 110 peak profiles are plotted in Fig. 3. (The curves have been normalized so that the area under each peak is the same.) Attention is drawn to two features of these curves. First, the peak for each film is shifted slightly (in 2Θ), indicating that the average lattice spacing in the direction normal to the plane of the film varies with sputter pressure. Second, the width (FWHM) of the peak increases with increasing sputter pressure. This latter effect is associated both with a decreasing grain size and with non-uniform strain (i.e. a distribution of lattice spacing). The strain may vary with depth or laterally or both.

The results of the $\sin^2\psi$ measurements are given in both Table 2 and Fig. 4. The cross-over from in-plane compression to tension, which in our films occurs just below 1 mTorr sputtering pressure, is a ubiquitous characteristic of sputtered thin-films [16].

Current thinking highlights the importance of film microstructure in determining the level of intrinsic stress present in polycrystalline thin-films [16,26–28]. When sputtering at high pressures, multiple gas-phase collisions reduce the energy of sputtered atoms and neutralized gas ions. In addition, the angle at which these incident species impact the substrate becomes more oblique. The resulting microstructure is characterized by porous columnar grain growth and significant intergranular voids. The observed increase in resistivity shown in Fig. 2 at higher sputtering pressure is a direct result of this sputtering induced porosity. Attractive forces (i.e. tensile forces between these grains) are inversely proportional in strength to the intergranular spacing. With decreasing pressure and less scattering of sputtered species, the films become less porous and more tightly packed. This results in both an increase in the in-plane tensile stress and a decrease in film resistivity. When the intergranular spacing decreases to a point where grains begin to touch (about 2 mTorr), compressive forces associated with atomic peening begin to exceed the above-mentioned tensile force. As this compressive force starts to increase, films exhibit a maximum in tensile stress and finally go into compression at very low sputtering pressures.

The existence of compression at higher pressures, seen in our films, is not often reported. Because film porosity should increase with sputtering pressure, the observed compressive force may be a casual effect associated with impurity absorption on the increased surface areas of the grains. Compressive forces resulting from the incorporation of O, H, and water vapor have previously been reported for a variety of metallic and dielectric thin-films [18,29,30]. In our case, the impurities are believed to be incorporated on the grain surface rather than in the bulk due to our efforts in minimizing contamination during film growth.

At first it might appear, when comparing the data shown in Figs. 3 and 4, that there is an increase in grain size with increasing pressure. For example, films with similar in-plane stress (and its related strain) but different line broadening should exhibit different size grains since line broadening is a convolution of both grain size and root-mean-square strain. Recent results using grazing incidence XRD have identified stress gradients in the depth direction as another potential cause of line broadening in other sputtered Mo films [31] at higher gas pressures. Deviations from linearity seen in d_{321} versus $\sin^2\psi$ plots for our films indeed support the presence of stress gradients perpendicular to the substrate in films sputtered at higher pressures. This could

explain why two films might have the same average level of in-plane stress (as determined by the $\sin^2\psi$ plot technique, a stress averaging technique) yet entirely different line broadening (due to differences in the stress gradient). Gradients may also be present in the in-plane directions.

Other Mo film properties that impact solar cell performance also varied with sputter pressure. In particular, the seven films exhibited different degrees of adhesion to the soda-lime glass substrates. This was immediately evident when as-deposited films were ultrasonically cleaned for less than 1 min in isopropyl alcohol. In some cases, pieces of the Mo film flaked off during this cleaning process. After cleaning, the degree of adhesion was qualitatively assessed using the "Scotch-tape test" [32]. Only those films deposited at the four highest pressures passed this test.

These results combined with the X-ray stress measurements yield an interesting observation. It appears that stress, as determined by the conventional $\sin^2\psi$ technique, may not be a good indicator of the adhesive quality of a polycrystalline thin-film. For example, films deposited at either extreme of the pressures investigated in this study were compressive in nature and of nearly identical magnitude, but were markedly different in regards to their adhesion to the glass substrates. The before-mentioned presence of stress gradients in our films may affect the integrity of the film and play a role in adhesion failure.

3.1. Mo bilayer process

As our results show, Mo films sputtered at a single pressure do not simultaneously possess low resistivity and good adhesion, both of which are desirable characteristics for fabricating back contact metallized layers for solar cells. In order to circumvent this problem, we have since designed an original two-pressure deposition scheme in which we first sputter a thin layer of "high-pressure" Mo to serve as an adhesion layer, followed by the deposition of "low-pressure" Mo to achieve low sheet resistance.

The procedure for fabricating the Mo bilayer was similar to that described earlier, except that the Ar pressure was varied during the deposition, as shown in Fig. 5. Sputtering was begun with the Ar pressure set to 10 mTorr. 2 min into the deposition, the gate-valve was manually opened in steps so as to achieve (nominally) a decrease in Ar pressure of 1 mTorr every 6 s, reaching a pressure of 1 mTorr after the third minute of deposition. The Ar pressure was maintained at 1 mTorr for the remainder of the deposition, and the sputter current control was adjusted to achieve $I = 1.0$ A at this lower pressure. This recipe has been used to routinely fabricate nominally 1.0 μm thick Mo films with sheet resistances in the range 0.12–0.14 $\Omega\ \square^{-1}$ (i.e. resistivities 12–14 μΩ cm) that pass the tape test for adhesion.

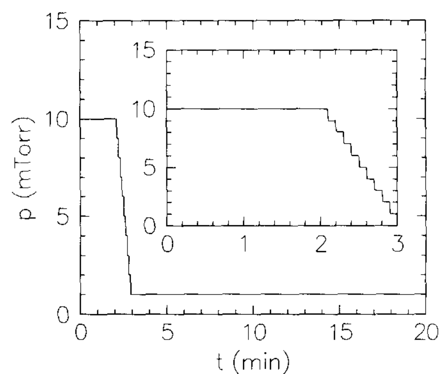

Fig. 5. Ar pressure versus time during the deposition of the Mo bilayer. The inset shows the pressure for the first 3 min of deposition.

We have fabricated other Mo bilayers by varying (a) the thicknesses of the high- and low-pressure layers, and (b) the value of the Ar pressure during deposition of the final, low-resistivity layer. The electrical properties of the resulting films are pretty much as expected, given their thicknesses and the resistivity values for the film layers in Table 1. A study is presently underway to investigate how these different Mo films hold up to the subsequent processing steps involved in fabricating the CIS and CIGS solar cells.

4. Conclusions

We have investigated the electrical and mechanical properties of seven Mo films sputtered onto soda-lime glass at different Ar pressures. The films investigated showed the following characteristics: (1) little change in resistivity (about 10 μΩ cm) from 0.2 to 2 mTorr followed by a steady increase above 2 mTorr; (2) films prepared at pressures greater than and equal to 2 mTorr passed the Scotch-tape adhesion test; (3) average in-plane residual stresses are compressive at 0.2 and 20 mTorr and passed through a maximum tensile value at about 2 mTorr, in agreement with Cuthrell et al. [24]. The stresses alone do not account for the adhesion behavior.

Finally, aided by the above observations, we have fabricated Mo bilayer films with the first layer sputtered at 10 mTorr and the second layer at 1 mTorr. These bilayer films pass the tape-test for adhesion and have low resistivities (12–15 μΩ cm).

Acknowledgments

The authors gratefully acknowledge M. Contreras, R. Noufi, J. Tuttle, and A. Gabor for useful discussions, and J. Dolan for his assistance with configuring the sputter system. This work was performed at NREL under contract No. DE-AC02-83CH10093 to the US

Department of Energy. Financial support for two of us (BB and PP) was provided by a seed grant from the Colorado Advanced Materials Group and partial support for one of us (JS) was furnished by an Associated Western Universities–Department of Energy faculty sabbatical fellowship.

References

[1] See, for instance, K. Zweibel, *Harnessing Solar Power: the Photovoltaic Challenge*, Plenum Press, New York, 1990; see also H.-W. Schock, *Mat. Res. Soc. Bull.*, *28* (1993) 42–44.
[2] M.A. Contreras et al., *Progr. Photovoltaics*, submitted.
[3] A.M. Gabor, J.R. Tuttle, D.S. Albin, A.L. Tennant, M.A. Contreras and R. Noufi, *Proc. 12th NREL P.V. Program Review Meeting, Oct. 13–15, 1993, Denver, CO*, AIP, 1994.
[4] F.A. Abou-Elfotouh et al., *J. Vac. Sci. Tech. A*, *8*(4) (1990) 3251–3254.
[5] S. Ashou et al., *Thin Solid Films*, *226* (1993) 129–134.
[6] R.J. Matson et al., *Solar Cells*, *11* (1984) 301–305.
[7] D.W. Niles et al., *Mat. Res. Soc. Symp. Proc.*, *260* (1992) 299–304.
[8] F.A. Abou-Elfotouh et al., *J. Vac. Sci. Technol.*, *7* (1989) 837–841.
[9] E. Moons et al., *J. Electron. Mater.*, *22*(3) (1993) 275–280.
[10] C.L. Chan and I. Shih, *J. Appl. Phys.*, *68*(1) (1990) 156–160.
[11] D.K. Rao et al., *Phys. Status Solidi*, *94* (1986) K153–K159.
[12] S. Raud and M.-A. Nicolet, *Thin Solid Films*, *201* (1991) 361–371.
[13] J.A. Thornton and D.W. Hoffman, *Thin Solid Films*, *171* (1989) 5–31.
[14] D.W. Hoffman and J.A. Thornton, *J. Vac. Sci. Technol.*, *20*(3) (1982) 355–358.
[15] J.A. Thornton and D.W. Hoffman, *J. Vac. Sci. Technol. A*, *3*(3) (1985) 576–579.
[16] T.J. Vink et al., *J. Appl. Phys.*, *70*(8) (1991) 4301–4308.
[17] B.L. Ballard, P.K. Predecki, D. Albin and J.H. Scofield, *Adv. X-Ray Anal.*, *38* (1994).
[18] T. Yamaguchi and R. Miyagawa, *Jpn. J. Appl. Phys.*, *30*(9A) (1991) 2069–2073.
[19] T. Bardin et al., *Thin Solid Films*, *165* (1988) 243–247.
[20] K. Kawabata et al., *Mat. Sci. Eng. A*, *163* (1993) 163–165.
[21] L. Krusin-Elbaum et al., *Thin Solid Films*, *153* (1987) 349–358.
[22] J.S. Lin et al., *Thin Solid Films*, *153* (1987) 359–368.
[23] A. Segmuller and M. Murakami, in K.N. Tu and R. Rosenberg (eds.), *Treatise on Materials Science and Technology*, Vol. 27, Academic Press, San Diego, CA, 1988, p. 197.
[24] R.E. Cuthrell, D.M. Mattox, C.R. Peeples, P.L. Dreike and K.P. Lamppa, *J. Vac. Sci. Technol. A*, *6*(5) (1988) 2914–2920.
[25] I.C. Noyan and J.B. Cohen, *Residual Stress: Measurement by Diffraction and Interpretation*, Springer–Verlag, New York, 1987, pp. 122–123.
[26] H. Windischmann, *Critical Rev. Solid State Mater. Sci.*, *17*(6) (1992) 547–596.
[27] K.-H. Muller, *J. Appl. Phys.*, *62* (1987) 1796–1799.
[28] M. Itoh, M. Hori and S. Nadahara, *J. Vac. Sci. Technol. B*, *9* (1991) 149–153.
[29] I. Blech and U. Cohen, *J. Appl. Phys.*, *53* (1982) 4202.
[30] H. Windischmann, R.W. Collins and J.M. Cavese, *J. Non-Cryst. Sol.*, *85* (1986) 261.
[31] B.L. Ballard, X. Zhu, P.K. Predecki and D.N. Braski, *Proc. 4th Int. Conf. on Residual Stresses*, Society of Experimental Mechanics, Baltimore, MD, 1994, pp. 1133–1143.
[32] D.S. Campbell, in L.I. Maissel and R. Glang (eds.), *Handbook of Thin Film Technology*, McGraw–Hill, New York, 1983, p. 12–16.